

# Ziegler-Nichols Based Controller Optimization for DFIG Wind Turbines

Farhat Nasim<sup>1</sup>, Shahida Khatoon<sup>1</sup>, Ibraheem<sup>1</sup>, \*Mohammad Shahid<sup>2</sup>, Shreya Baranwal<sup>1</sup>, Sajad Ahmad Wani<sup>1</sup>

<sup>1</sup>Department of Electrical Engineering, Faculty of Engineering and Technology, Jamia Millia Islamia, New Delhi, India

<sup>2</sup>Department of Electrical Engineering, Galgotias College of Engineering and Technology, Greater Noida, India

**Abstract:** Wind power conversion systems are becoming the most preferable alternate renewable energy source. Doubly Fed Induction Generator's utilization rotating parts in wind turbines is increasing with the wind power penetration to the electric grid. The observation becomes more noticeable when there are abnormal conditions within the electrical power system. In this paper, MPPT Controller is incorporated with DFIG through the MATLAB Simulink program is simulated. A conventional PI controller is tuned with Ziegler-Nichol's (Z-N) method and was implemented to the DFIG Control Block. The rotor-side converter (RSC) is utilized to regulate the power generated by the doubly-fed induction generator (DFIG), while the direct current (DC) bus voltage is controlled by the grid-side converter (GSC). The DFIG's angular and comparative angular speeds are used to generate the reference torque value in the MPPT controller. This improved the time response, output power, electromotive torque, and other current and voltage characteristics. A comparison was made between the output evaluation of the inbuilt controller and the output evaluation of the proposed controller. The MPPT with tuned PI Controller's results show that the suggested system, which uses DFIG coupled to a rotor, is accurate, dependable, and feasible.

**Keywords**— Wind power conversion systems, Rotor converter (RC), Maximum Power Point Controller (MPPT), Ziegler-Nichols (Z-N), PI Controller, Dual-fed wound rotor induction generator (DFIG), etc.

## Introduction

Wind power generation has been growing continuously in recent years. Renewable energy sources replace conventional methods to generate electricity, mainly due to their non-polluting nature and cost-effectiveness. Environmental risks, including air pollution and greenhouse gas emissions, are growing globally. As environmental worries grow, the importance of wind energy conversion system has been increased. By adjusting the dynamics of a wind turbine operating under varying wind speed conditions while enabling the system to quickly respond to changes in wind speed, this paper considers a crucial requirement of WECS: generating the desired power [1].

The advancement and widespread use of wind turbines in modern times has prompted electrical engineering researchers to carry out studies aimed at enhancing electromechanical conversion efficiency and energy quality. DFIG is mainly applied in the case of variable-speed wind turbines (VSWT) that use a fixed inverter coupled to the stator and rotor. Around 50% of wind power Conversion System (WECS) technologies use this strategy. Double-fed induction generators are highly desirable for these applications because they can generate a controlled high power because of their lower-rated power converters compared to other wind generator technologies. Because of its various benefits over other turbines, DFIG is the most ideal generator employed in WECS [2].

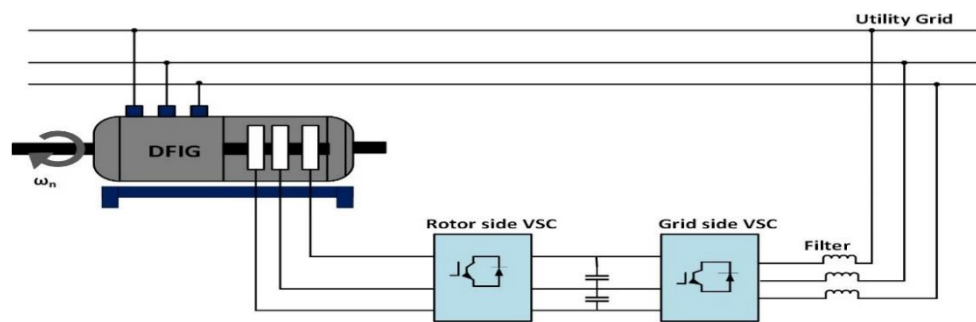


**Fig. 1. Simplified design of the power system relying on wind energy generation with DC link Capacitor [3].**

Figure 1 depicts a simplified design of the power system relying on wind energy generation. The Scherbius topology refers to this configuration, which also includes a gearbox, DFIG, wind turbine, and a DC capacitor connecting the two voltage-source inverters. The network is connected to the stator circuit in three ways: directly through the stator circuit, via brushes and slip rings to the rotor windings, and via a harmonic filter to the converter on the grid side [3].

The DFIG's speed control has two modes of operation, as specified in [4]. The first mode happens when the wind speed is lower than the designated value, causing the generator to operate slower than the synchronous speed, resulting in a positive slip. In this situation, the rotor winding and the grid are supplied with electricity through the stator winding. In the second mode, the rotor speed surpasses the synchronous speed, resulting in a negative slip. In this case, electrical power is transmitted to the grid using the generator's stator and rotor windings. To ensure that the generator speed remains close to its rated value, it is crucial for the parameters of the generator speed controller to be capable of self-adjustment, considering the variable nature of actual wind speed.

Ziegler-Nichol's algorithm is one of the most popular tuning techniques. The PI parameters can be found using this approach without any mathematical calculations. To simulate changing speed wind turbines utilizing the MPPT method, this article aims to create the model and vector control of such turbines within the MATLAB/SIMULINK environment. The conversion system simulation and modeling (turbine and DFIG) were first. Next, stator vector control of active and reactive powers was suggested [5]. Finally, to enhance response time and guarantee alignment with the DFIG power curve, MPPT control was integrated into the RSC. Systems for converting renewable energy, including PV systems and WECS, frequently use MPPT algorithms. Getting the most power possible from the WECS is the primary goal of this strategy. More accurate reference torque ( $T_{em}^*$ ) values will be obtained when compared to the inbuilt PI controller produced with the Maximum Power Point Tracker controller introduced to the RSC. In this approach, the system's response time was shortened, and the desired level of power generation was attained. Rotor speed, Torque, Stator, and Rotor current and voltage characteristics were utilized to compare the suggested system's performance with a conventional PI controller utilizing MPPT control with PI.

Research Methodology Includes:

- Develop and build a Doubly Fed Induction Generator (DFIG) model using mathematical equations. Incorporate controllers within the model to obtain responses for various wind speed.
- A traditional PI controller was calibrated using the Ziegler-Nichols (Z-N) technique and applied to both the rotor and grid-side converters.
- The Maximum power point controller, in conjunction with the calibrated PI controller, was utilized to produce set values for the rotor-side and grid-side parameters.

The suggested controller enhanced the speed of response, reactive power, electromagnetic torque, and grid-side current parameters. This paper is divided into 5 sections: Section 1, which introduces DFIG system modeling; Section 2, which briefly describes the modeling of DFIG; and Section 3, which discusses controlling rotor and grid side converters. Results and Discussion in Section 4 and conclusion in section 5.

## 2. Description of the modeling and wind conversion system

### A. Aerodynamic Model

By determining the Mechanical torque of the airflow on the blades, the rotor's power extraction is simulated using the aerodynamic model. The wind speed, incidence, and torque on the low-speed shaft can be determined using wind speed along the rotors' swept region. The following expression [6] defines the torque that the rotor generates:

We must apply the following expression to define mechanical power [7].

$$P_m = \frac{1}{2} \rho \pi R^2 V^3 C_p(\lambda, \beta) \quad (1)$$

As determined, the tip speed ratio was:

$$\lambda = \frac{\Omega_t R}{v} \quad (2)$$

The  $C_p$  value for a wind turbine rotor with variable speed can be approximated using the following expression:

$$C_p(\lambda, \beta) = C_1 \left( \frac{C_2}{\lambda_i} - C_3 \beta - C_4 \beta^{C_5} - C_6 \right) e^{\left( \frac{-C_7}{\lambda_i} \right)} \quad (3)$$

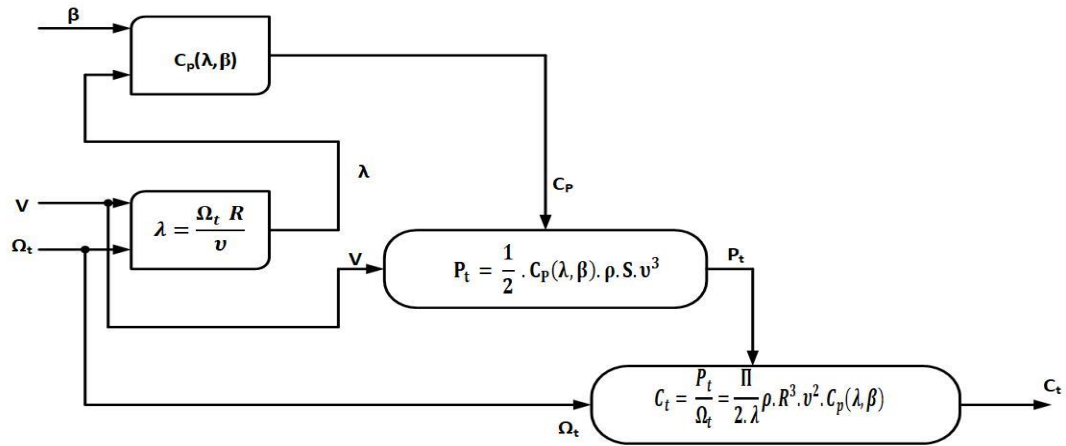


Fig.2 Wind turbine Aerodynamic model [6, 10].

The mechanical energy caused the rotor to revolve rapidly, producing aerodynamic torque. The aerodynamic torque in Figure 3 can be stated as follows:

$$T_t = \frac{P_t}{\Omega_t} = \frac{\pi}{2\lambda} \rho \cdot R^3 \cdot V^2 \cdot C_p(\lambda, \beta) \quad (4)$$

### B. Dynamic Modelling of DFIG

A rotating three-phase phasor makes it challenging to run an AC machine continuously. When a reference frame rotates at the same speed as the stator flux, a three-phase (ABC) system can be split into two phases (d-q) using the Park's transformation [11]. Equations for flux are expressed as follows in terms:

$$\dot{\Psi}_{ds} = \Re_s \Im_{ds} + \frac{d\Psi_{ds}}{dt} - \omega_e \Psi_{qs} \quad (5)$$

$$\dot{\Psi}_{qs} = \Re_s \Im_{qs} + \frac{d\Psi_{qs}}{dt} - \omega_e \Psi_{ds} \quad (6)$$

$$\dot{\Psi}_{dr} = \Re_r \Im_{dr} + \frac{d\Psi_{dr}}{dt} - (\omega_e - \omega_r) \Psi_{qr} \quad (7)$$

$$\dot{\Psi}_{qr} = \Re_r \Im_{qr} + \frac{d\Psi_{qr}}{dt} + (\omega_e - \omega_r) \Psi_{dr} \quad (8)$$

To calculate electromagnetic torque.

$$\tau_e = \frac{3}{2} \left( \frac{P}{2} \right) \frac{1}{\omega_b} (\Psi_{ds} \mathfrak{T}_{qs} - \Psi_{qs} \mathfrak{T}_{ds}) \quad (9)$$

$$\tau_e - \tau_L = \int \frac{2}{P} \frac{d\omega_r}{dt} \quad (10)$$

$$P_s = \frac{3}{2} (\gamma_{ds} \mathfrak{T}_{ds} + \gamma_{qs} \mathfrak{T}_{qs}) \quad (11)$$

$$Q_s = \frac{3}{2} (\gamma_{qs} \mathfrak{T}_{ds} - \gamma_{ds} \mathfrak{T}_{qs}) \quad (12)$$

**Table 1: Referred Parameter to rotor side**

Parameter	Symbol	Values
Rated Stator-Power	( $P_s$ )	$2 \times 10^6$ W
Stator Frequency	(f)	50Hz
Stator (Voltage, Current)	( $\gamma_s$ ), ( $\mathfrak{T}_s$ )	690V, 1.76KA
Rotor Voltage	( $\gamma_r$ )	2070V
Stator Resistance, Leakage Inductance	( $\mathfrak{R}_s$ ), ( $L_s$ )	2.65 m $\Omega$ , 0.0026H
Inductance Stator		
Rotor Resistance, Leakage Inductance	( $\mathfrak{R}_r$ ), ( $L_r$ ), ( $L_m$ )	2.91 m $\Omega$ , 0.00269H, 2.5mL
Rotor, Magnetizing-Inductance		

**Table 2: Referred Parameters to stator side**

Parameters	Symbol
Mag flux of d-q axis	( $\Psi_{md}$ , $\Psi_{mq}$ )
stator and rotor voltages of the d-q axis	( $\gamma_{ds}$ , $\gamma_{dr}$ ), ( $\gamma_{qs}$ , $\gamma_{qr}$ )
stator and rotor currents of the d-q axis	( $\mathfrak{T}_{qs}$ , $\mathfrak{T}_{qr}$ ), ( $\mathfrak{T}_{ds}$ , $\mathfrak{T}_{dr}$ )
Stator and rotor side Reactance	( $\chi_{ls}$ ), ( $\chi_{lr}$ )
Angular frequency, Rotor speed.	( $\omega_e$ ), ( $\omega_r$ )
Base angular frequency	( $\omega_b$ )

**Table 3: Parameters for Grid Controller**

Parameter	Symbol	Values
dc bus Voltage	$\gamma_{bus}$	325.27V
dc bus capacitance	C <sub>bus</sub>	0.0800F
Grid filter Resistance	$\mathfrak{R}_s$	$2 \times 10^{-5} \Omega$
Grid Inductance Resistance	$L_s$	$40 \times 10^{-5} H$

**Table 4: Parameters for Wind Turbine**

Parameter	Symbol	Values
Density of Air	$\rho$	1.225kg/m <sup>3</sup>
Radius	R	42m
Gearbox Ratio	N	1:100
Rated Wind Speed	V	12m/s

### 3. Control Techniques

#### A) Implementation of the Ziegler-Nichols method for PI Controller Tuning

This section highlights the implementation of Proportional-Integral (PI). The aim is to evaluate and compare the effectiveness of this control design strategy in terms of response time, tracking accuracy, overshoot, and stability under various operating conditions. The proposed controller was designed, simulated, and tested to ensure the reliable performance of the strategy. The Proportional-Integral (PI) controller is a traditional control strategy primarily used in control system applications for its simplicity and effectiveness. The method systematically tunes PI controllers to achieve desired stability and response time performance characteristics.[12-16]

1. **System Identification:** The first step is identifying the system for which the PID controller must be tuned. This involves understanding the system's dynamics, transfer function, and response to different inputs.
2. **Proportional Gain (Kp) Adjustment:** Initially, the integral term of the PI controller is set to zero, and the proportional gain (Kp) is adjusted. The proportional gain is continuously raised until the system reaches a state of steady oscillation or sustained oscillation.
3. **Oscillation Characteristics:** Once the system starts to oscillate, the amplitude and period of the oscillations are measured. The amplitude is the peak-to-peak distance of the oscillations, and the period is the time taken for one complete oscillation cycle.
4. **Calculate Ultimate Gain (Ku) and Ultimate Period (Tu):** Using the amplitude and period of the oscillations, the ultimate gain (Ku) and ultimate period (Tu) are calculated. Ku is the proportional gain value at which the system exhibits sustained oscillations, and Tu is the corresponding period.
5. **PI Controller Tuning:** Based on the values of Ku and Tu, the PI controller parameters are determined using predefined tuning rules. The Ziegler-Nichols method suggests specific parameter values depending on the PI Controller: **PI (Proportional-Integral) Controller:**  $K_p = 0.45 * K_u$ ,  $T_i = T_u / 1.2$
6. **Fine-Tuning:** After setting initial PID parameters based on the Ziegler-Nichols method, further adjustments may be made based on system performance requirements and stability considerations. The

The activation and reversing power supply are regulated by vector controls located on the converters on the rotor side. The block diagram of the RSC controller is depicted in Figure 3. The rotor-side converter is used to control the stator flux in a field-oriented vector manner. Reactive power can be controlled using direct axes loops, whereas active power can be controlled using quadrature axes loops.

The process of DFIG control starts with the formation of the GSC using Matlab/Simulink. The previous part discussed the conversion equations and equivalent circuits applied to developing GSC. This control strategy ensures the stability of the DC bus voltage by generating a sinusoidal current that matches the frequency of the DC bus. To get a power factor of unity, a ref value of zero reactive power is established. The control approach that was used is shown in Figure 4. The control technique includes two loops: one for voltage regulation and another for current regulation. Through a filter, ( $L_s, R_s$ ) connections are made to the electrical grid from the rotor side [17].

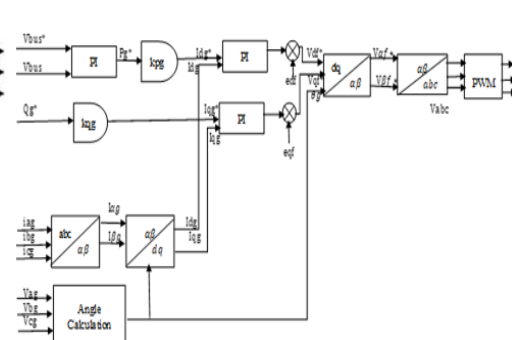


#### Fig.4 Grid Side Controller

Equations for formulating Grid Side Converter (GSC) are:

$$V_{s_a} = V_{s_a} - R_s i_{s_a} - L_s \frac{di_{s_a}}{dt} \quad (13)$$

$$V_{s_b} = V_{s_b} - R_s i_{s_b} - L_s \frac{di_{s_b}}{dt} \quad (14)$$

$$V_{s_c} = V_{s_c} - R_s i_{s_c} - L_s \frac{di_{s_c}}{dt} \quad (15)$$

$$V_{sd} = V_{sd} - R_s i_{sd} - L_s \frac{di_{sd}}{dt} + E_{sq} \quad (16)$$

$$V_{sq} = V_{sq} - R_s i_{sq} - L_s \frac{di_{sq}}{dt} + E_{sd} \quad (17)$$

Powers with the grid are:

$$P_s = V_{sq} i_{sq} = \frac{3}{2} V_s i_{sd} \quad (18)$$

$$Q_s = V_{sd} i_{sd} = \frac{3}{2} V_s i_{sq} \quad (19)$$

### B.1 Current Controlling loop for Rotor Side Converter

The block diagram below depicts the comparable representation of the closed-loop current regulation in the rotor-side control block, as cited from reference [24].

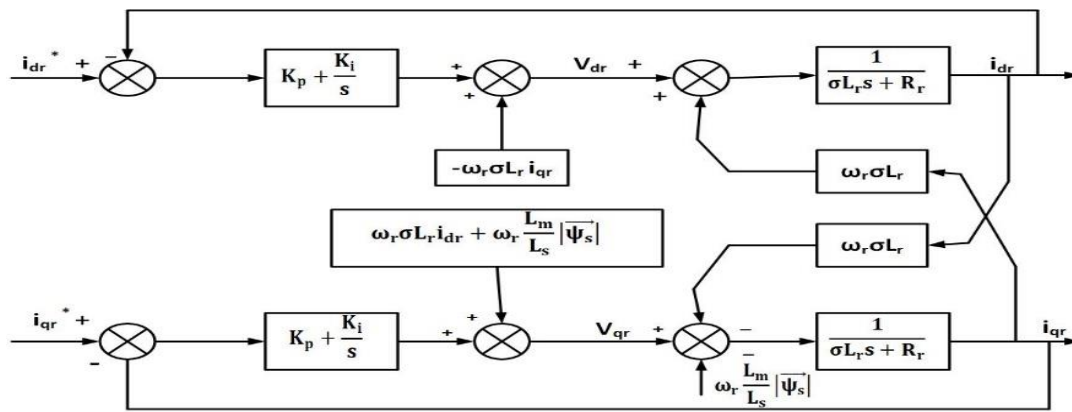


Fig.5 Inner Current controlling Loop for RSC [24]

The block diagram depicted above can be reduced into the transfer function as follows:

$$\frac{i_{ds}(s)}{i_{ds}^*(s)} = \frac{sk_p + k_i}{s^2 L_r \sigma + s(R_r + k_p) + k_i} \quad (20)$$

$$\frac{i_{qs}(s)}{i_{qs}^*(s)} = \frac{sk_p + k_i}{s^2 L_r \sigma + s(R_r + k_p) + k_i} \quad (21)$$

Next, we compare the given transfer function with the denominator of the general control transfer function, which is a second-order polynomial in the form of  $s^2 + 2\xi\omega_n s + \omega_n^2$  we have,

$$k_i = L_r \cdot \sigma \omega_n^2 \text{ and } k_p = 2 \cdot L_r \cdot \xi \omega_n - R_r \quad (22)$$

This comparison allows us to determine gain constants for the PI controller. By using these kp and ki gains values, the Transfer Function will come out to be

$$= \frac{3373.1295s + 2858668.32}{s^2 + 3384.9463s + 2858668.32} \quad (23)$$

### C. Maximal Extraction of Power

Variable speed operation is achieved through the control technology of the DFIG wind turbine, optimizing output power over various wind speeds. The maximum possible wind power generation is attained by adjusting the rotor speed to match the power coefficient. To ensure that the turbine blade can harness the most wind power potential, we must adapt the tip speed ratio to its ideal level, as shown in Fig 6. In this case, the optimization constant is Kopt, and the gearbox ratio is N. The definition of Kopt is as follows:

#### D. Rotor-Side Converter (RSC) Control with Proposed Strategy

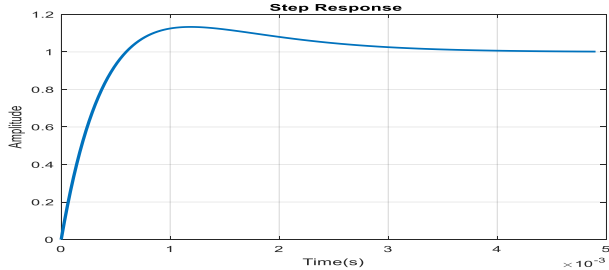
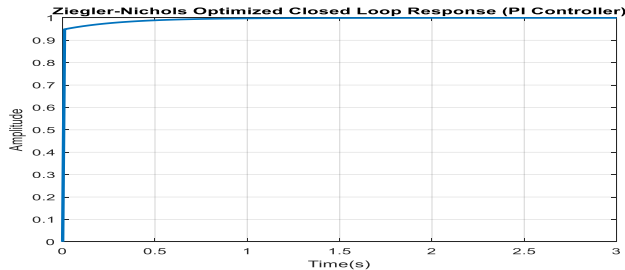
The block diagram illustrates the control system for a three-phase inverter. It starts with reference inputs  $i_{dr}^*$ ,  $\omega_m^*$ , and  $\omega_m$ .  $\omega_m^*$  and  $\omega_m$  are processed by an MPPT block to produce  $T_{em}^*$ , which is then multiplied by a gain  $K$  to produce  $i_{qr}^*$ .  $i_{dr}^*$  and  $i_{qr}^*$  are each fed into a PI controller. The outputs of these PI controllers are summed with feedback terms  $-\omega_r \sigma L_r i_{qr}$  and  $\omega_r (\sigma L_r + i_{ms} L_m / L_s)$  to produce  $V_{dq}^*$  and  $V_{qd}^*$ . These voltage references are then transformed from the dq frame to the  $\alpha\beta$  frame using a  $dq \rightarrow \alpha\beta$  block. The resulting  $V_{\alpha f}^*$  and  $V_{\beta f}^*$  are transformed from the  $\alpha\beta$  frame to the abc frame using an  $\alpha\beta \rightarrow abc$  block, yielding  $V_a^*$ ,  $V_b^*$ , and  $V_c^*$ . These voltage references are then processed by a PWM block to generate the final output signals  $S_{a,r}$ ,  $S_{b,r}$ , and  $S_{c,r}$ . The diagram also shows the transformation of input currents  $i_{ar}$ ,  $i_{br}$ , and  $i_{cr}$  from the abc frame to the  $\alpha\beta$  frame, and then to the dq frame using an  $\alpha\beta \rightarrow dq$  block. The output of this block provides feedback signals  $i_{qr}$  and  $\theta_r$  to the control system. An Angle Calculation block also provides  $\theta_r$  to the  $dq \rightarrow \alpha\beta$  block.

The MPPT controller that is introduced to the RSC primarily aims to increase the electromagnetic torque, grid current, and WECS reaction time by generating a more precise Reference Torque than the PI controller. Figure 7 shows the MPPT controller built using the Matlab/Simulink environment.

A comparison of the proposed and inbuilt model by implementing the tuned PI Controller into the system is shown in Table 5 and Table 6. These  $k_p$  and  $k_i$  gains used in the proposed model along with MPPT Controller for desired response. By tuning with the Ziegler Nichol's method the rise time decreases, settling time decreases and overshoot reduces from 13% to 3% as shown in table 6.



Table. 5. Comparison of Responses and Gains for PI Controller

Tuning	Response
<p><b>Before tuning the PI Controller</b></p> <p><b>Kp = 0.58 and Ki= 491.6 [23]</b></p> <p><b>Transfer Function =</b>  <math display="block">\frac{3373.1295s + 2858668.32}{s^2 + 3384.9463s + 2858668.32}</math></p>	
<p><b>After tuning with Ziegler- Nichol's</b></p> <p><b>Kp = 4.1 and Ki = 2.50</b></p> <p><b>The transfer function of the system will be</b>  <math display="block">\frac{23984.6s + 14546.72}{s^2 + 24001.51s + 14546.72}</math></p>	

PARAMETERS	BEFORE TUNING GAINS VALUES	AFTER TUNED WITH ZIEGLER NICHOLS METHOD
KP (PROPORTIONAL GAIN)	0.58	<b>6.122</b>
KI (INTEGRAL GAIN)	491.6	<b>2.5</b>
Tr (RISE TIME) sec	0.000 434	#####
Ts (SETTLING TIME) sec	0.0032	#####
OVERSHOOT(%)	13.3246	<b>3</b>

Table. 6. Comparison of Transient Performance Parameters and Gains for PI Controller

Implementing a control strategy for wind turbines utilizing Dual Fed Induction Generator (DFIG) is carried out using MATLAB/SIMULINK. The simulation results are presented below. Simulink is utilized to replicate Doubly Fed Induction Generators (DFIGs) with four magnetic poles. These DFIGs operate at a voltage of 690V and a frequency of 50Hz while delivering a power output of 2.4MW.

Figure 8 illustrates the simulated response of the actual rotor speed tracking about the variability in wind speed. Fig 9 illustrates that the proposed PI with MPPT controller achieves a quadrature current from the Rotor side that is better than the inbuilt PI controller. The evaluation of the system architecture also included an assessment of the DC bus voltages. Figure 10 and Figure 11 depict the graphical depiction of the planned system's DC bus



voltage using the regular PI controller and the suggested Proposed controller. The graph shows the variation of the DC bus voltage at different wind speeds. Compared to these experiments, the proposed PI with MPPT DFIG-based WECS demonstrates a quicker response time in tracking the reference DC bus voltage under varying wind speeds.

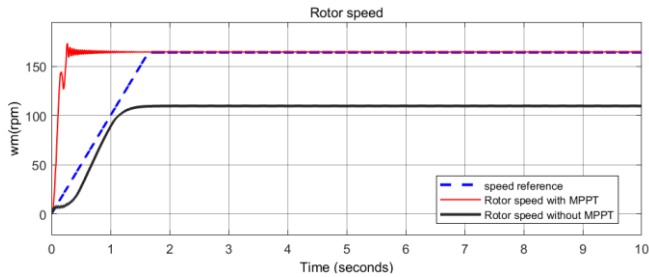


Fig. 8 Rotor speed when connected with MPPT and PI

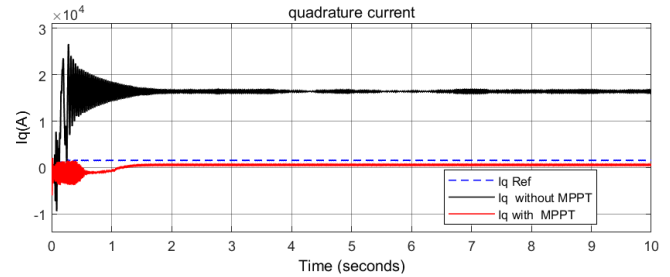


Fig.9 Quadrature Current when MPPT and PI connected

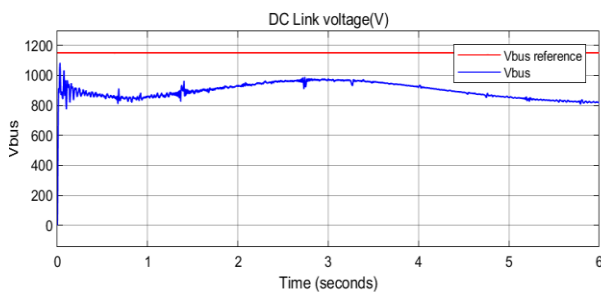


Fig. 10 DC Link Voltage When PI Connected

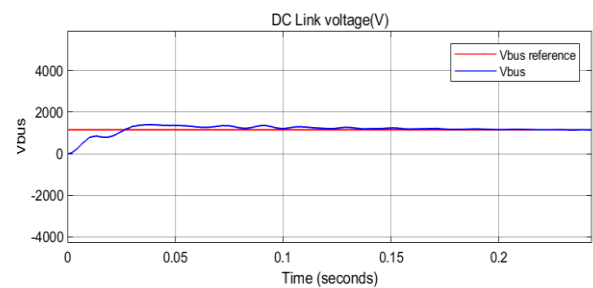


Fig.11 DC Link Voltage When Proposed MPPT with PI

Figure 12 and Figure 13 show the direct axis current with the desired Reference Value achieved by the proposed model. Furthermore, the suggested system underwent analysis from the perspective of electromagnetic torque ( $T_{em}$ ). Figure 14 and Figure 15 display the graphical representation of the electromagnetic torque ( $T_{em}$ ) for both the inbuilt and the proposed controller. The torque of the DFIG achieved the desired level more quickly with the assistance of the Proposed controller than the inbuilt controller. The Proposed controller successfully adhered to the specified torque value.

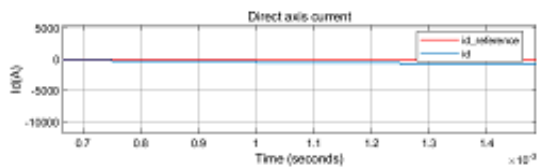


Fig. 12 Direct axis current when PI Connected

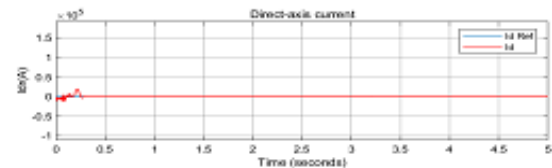


Fig.13 Direct axis Current When proposed MPPT with PI

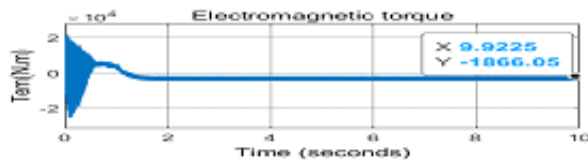


Fig. 14 Electromagnetic torque when PI connected

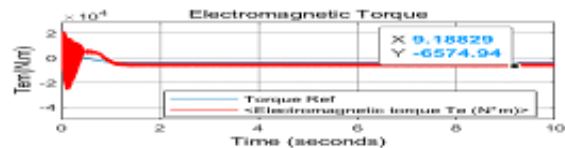


Fig. 15 Electromagnetic torque when PI and MPPT

Table 6. Comparison of the in-built Controller and the Proposed Controller

<i>S. No</i>	<i>Parameters</i>	<b>PI Controller without MPPT</b>	<b>Proposed Controller (MPPT with PI)</b>
1.	Rotor speed	110 <i>rad/s</i>	172 <i>rad/s</i>
2.	Electromagnetic Torque	-1866N.m	-6574N.m
3.	Generated Power	$110 \times (1866) = 0.2\text{MW}$	$172 \times (6574) = 1.15\text{MW}$
4.	Response time	2.00s	0.85s

## 5. Conclusion

A simulation was performed on a grid-connected dual-fed induction generator (DFIG) based on a wind energy power system. At first, the mathematical models for the turbine and DFIG were suggested. The study sought to assess the durability of a calibrated PI controller across the wide range of operating conditions of a DFIG-based wind energy harvesting system, providing objective and quantitative results to illustrate its performance attributes. The design models for the controller and the mechanical, aerodynamic, electrical, and control systems of the proposed DFIG were simulated using MATLAB-SIMULINK. The purpose of this was to assess the effectiveness of the simulated PI controller in the overall system design model. At first, a built-in PI controller was employed on the rotor converter to regulate the current and voltages on the d and q axes of both converters. After using the proposed controller, the rotor speed and electromagnetic torque increases resulting in increasing the generated Power as shown in Table 6.

Nevertheless, the outcomes indicated that the PI controller failed to attain the desired reference values and displayed increased oscillations. As a result, the built-in PI controller was calibrated using the Ziegler-Nichols technique. In addition, an MPPT controller was integrated into both the rotor and grid side converters to enhance the WECS's response time and attain the targeted power output. The voltage and current waveforms of the stator were both balanced and sinusoidal. The simulation analysis demonstrated that the proposed system, when implemented with the control approach, achieved satisfactory performance, and exhibited excellent results and reduces the rise time, delay time and overshoot percentage.

## References

- [1] Prakash Bharti, O. (2024). Optimization Techniques of DFIG Controller Design for Wind Energy Conversion Systems. <https://doi.org/10.21203/rs.3.rs-3942454/v1>.
- [2] Patel, R., Hafiz, F., Swain, A., & Ukil, A. (2021). Nonlinear rotor side converter control of DFIG based wind energy system. *Electric Power Systems Research*, 198. <https://doi.org/10.1016/j.epsr.2021.107358>
- [3] Giri, J., Mishra, N. K., Patra, A., & Shukla, M. K. (2024). Control Strategies of DFIG Technology-based Variable-Speed Wind Turbines- A Review. *IOP Conference Series: Earth and Environmental Science*, 1285(1). <https://doi.org/10.1088/17551315/1285/1/012007>.
- [4] Bekiroglu, E., & Yazar, M. D. (2022). MPPT Control of Grid Connected DFIG at Variable Wind Speed. *Energies*, 15(9). <https://doi.org/10.3390/en15093146>.
- [5] F. Nasim, S. Khatoon, I. Ibraheem, M. Shahid and M. F. Ahmer, "Effect of PI Controller on Power Generation in Double-Fed Induction Machine," 2022 4th International Conference on Advances in Computing, Communication Control and Networking (ICAC3N), Greater Noida, India, 2022, pp. 2418-2424, doi: 10.1109/ICAC3N56670.2022.10074573.
- [6] Xu, L., & Wang, Y. (2007). Dynamic modeling and control of DFIG-based wind turbines under unbalanced network conditions. *IEEE Transactions on Power Systems*, 22(1), 314–323. <https://doi.org/10.1109/TPWRS.2006.889113>.

- [7] Hete, R. R., Shrivastava, T., Dash, R., Anupallavi, L., Fathima, M., Reddy, K. J., Dhanamjayalu, C., Mohammad, F., & Khan, B. (2024). Design and development of PI controller for DFIG grid integration using neural tuning method ensembled with dense plexus terminals. *Scientific Reports*, 14(1). <https://doi.org/10.1038/s41598-024-56904-7>
- [8] Meera, G. S., and N. A. Divya. "Rotor side converter control of DFIG based wind energy conversion system." *Int J Eng Res Technol (IJERT)* 4 (2015): 607-612.
- [9] F. Nasim, S. Khattoon, Ibraheem and M. Shahid, "Field Control Grid Connected DFIG Turbine System," 2023 International Conference on Power, Instrumentation, Energy and Control (PIECON), Aligarh, India, 2023, pp. 1-5, doi: 10.1109/PIECON56912.2023.10085726.
- [10] Vas, Peter. *Sensorless vector and direct torque control*. Vol. 42. Oxford,[Eng.]; New York: Oxford University Press, 1998.
- [11] Chatterjee, Debjyoti, and Zakir Hussain Rather. "Modelling and Control of DFIG-based Variable Speed Wind Turbine." (2018).
- [12] Bharti, O. P., Sarita, K., Vardhan, A. S. S., Vardhan, A. S. S., & Saket, R. K. (2021). Controller design for DFIG-based WT using gravitational search algorithm for wind power generation. *IET Renewable Power Generation*, 15(9), 1956–1967. <https://doi.org/10.1049/rpg2.12118>
- [13] Behera, M. P. (2024). Mathematical Modeling of DFIG Based Wind Energy Conversion System. In *International Journal of Creative Research Thoughts* (Vol. 12). [www.ijcrt.org](http://www.ijcrt.org)
- [14] Abad, Gonzalo, Jesus Lopez, Miguel Rodriguez, Luis Marroyo, and Grzegorz Iwanski. *Doubly fed induction machine: modeling and control for wind energy generation*. John Wiley & Sons, 2011.
- [15] Singh, P., Arora, K., & Rathore, U. C. (2022). Control Strategies for Improvement of Power Quality in Grid Connected Variable Speed WECS with DFIG – An Overview. *Journal of Physics: Conference Series*, 2327(1), 012008. <https://doi.org/10.1088/1742-6596/2327/1/012008>
- [16] Novaes Menezes, E. J., Araújo, A. M., & Bouchonneau da Silva, N. S. (2018). A review on wind turbine control and its associated methods. In *Journal of Cleaner Production* (Vol. 174, pp. 945–953). Elsevier Ltd. <https://doi.org/10.1016/j.jclepro.2017.10.297>
- [17] Li, P., Song, Y. D., Li, D. Y., Cai, W. C., & Zhang, K. (2015). Control and monitoring for grid-friendly wind turbines: Research overview and suggested approach. *IEEE Transactions on Power Electronics*, 30(4), 1979–1986. <https://doi.org/10.1109/TPEL.2014.2325869>
- [18] Knight, A. M., & Peters, G. E. (2005). Simple wind energy controller for an expanded operating range. *IEEE Transactions on Energy Conversion*, 20(2), 459–466. <https://doi.org/10.1109/TEC.2005.847995>
- [19] Alam, S., & Rathore, P. K. (n.d.). Simulation, Modeling and Control of a Doubly Fed Induction Generator Base Wind Turbine System-A Review. *International Journal of Trend in Innovative Research*. [www.ijtiir.com](http://www.ijtiir.com)
- [20] Xia, Y., Ahmed, K. H., & Williams, B. W. (2013). Wind turbine power coefficient analysis of a new maximum power point tracking technique. *IEEE Transactions on Industrial Electronics*, 60(3), 1122–1132. <https://doi.org/10.1109/TIE.2012.2206332>
- [21] Aktarujjaman, M., Md Enamul Haque, K. M. Muttaqi, M. Negnevitsky, and G. Ledwich. "Control Dynamics of a doubly fed induction generator under sub-and super-synchronous modes of operation." In *2008 IEEE Power and Energy Society General Meeting-Conversion and Delivery of Electrical Energy in the 21st Century*, pp. 1-9. IEEE, 2008.
- [22] Tang, Choon Yik, Yi Guo, and John N. Jiang. "Nonlinear dual-mode control of variable-speed wind turbines with doubly fed induction generators." *IEEE Transactions on Control Systems Technology* 19, no. 4 (2010): 744-756.
- [23] K. A.-H. Haitham Abu-Rub, Mariusz Malinowski, Ed., *Power Electronics for renewable Energy Systems, Transportation and Industrial Applications*, First. IEEE Press and John Wiley & Sons Ltd.
- [24] G. Abad, *Power Electronics and Electric Drives for Traction Applications*. 2016.
- [25] Tarek Medalel Masaud and P. K. Sen, "Modeling and control of doubly fed induction generator for wind power," 2011 North American Power Symposium, 2011, pp. 1-8, doi: 10.1109/NAPS.2011.6025122.

- 
- [26] Pena, Ruben, J. C. Clare, and G. M. Asher. "Doubly fed induction generator using back-to-back PWM converters and its application to variable-speed wind-energy generation." *IEE Proceedings-Electric power applications* 143, no. 3 (1996): 231-241.
- [27] J. Vidal, G. Abad, J. Arza and S. Aurtenechea, "Single-Phase DC Crowbar Topologies for Low Voltage Ride Through Fulfillment of High-Power Doubly Fed Induction Generator-Based Wind Turbines," in *IEEE Transactions on Energy Conversion*, vol. 28, no. 3, pp. 768-781, Sept. 2013, doi: 10.1109/TEC.2013.2273227.
- [28] M. Liserre, R. C'ardenas, M. Molinas, aJ. Rodr'iguez, "Overview of multi-MW wind turbines and wind parks," *IEEE Trans. Ind. Electron.*, vol. 58, no. 4, pp. 1081–1095, Apr. 2011.
- [29] Y. Jun, L. Hui, L. Yong, and C. Zhe, "An improved control strategy of limiting the DC-link voltage fluctuation for a doubly fed induction wind generator," *IEEE Trans. Power Electron.*, vol. 23, no. 3, pp. 1205–1213, May 2008.
- [30] M. Mohseni, S. M. Islam, and M. A. S. Masoum, "Impacts of symmetrical and asymmetrical voltage sags on DFIG-based wind turbines considering phase-angle jump, voltage recovery, and sag parameters," *IEEE Trans. Power Electron.*, vol. 26, no. 5, pp. 1587–1598, May 2011.
- [31] C. Wessels, F. Gebhardt and F. W. Fuchs, "Fault Ride-Through of a DFIG Wind Turbine Using a Dynamic Voltage Restorer During Symmetrical and Asymmetrical Grid Faults," in *IEEE Transactions on Power Electronics*, vol. 26, no. 3, pp. 807-815, March 2011, doi: 10.1109/TPEL.2010.2099133.
- [32] Chen, Z. J., & Stol, K. A. (2014). An assessment of the effectiveness of individual pitch control on upscaled wind turbines. *Journal of Physics: Conference Series*, 524(1). <https://doi.org/10.1088/1742-6596/524/1/012045>